Scientia Iranica (2024) 31(10), 775–789

Sharif University of Technology
Scientia Iranica
Transactions D: Computer Science & Engineering and Electrical Engineering
https://scientiairanica.sharif.edu

Fault-tolerant capability analysis of six-phase induction motor with distributed, concentrated, and pseudo-concentrated windings

M. Alemi-Rostami[a], G. Rezazadeh[b,*], F. Tahami[c], and H.R. Akbari-Resketi[d]

a. *Department of Electrical Engineering, Khayam Research Institute (KRI), Ministry of Science, Research, and Technology, Tehran, Iran.*
b. *School of Electrical and Computer Engineering, College of Engineering, University of Tehran, Tehran, Iran.*
c. *Department of Electrical Engineering, Sharif University of Technology, Tehran, Iran.*
d. *Department of Electrical and Computer Engineering, Babol Noshirvani University of Technology, Babol, Iran.*

Received 7 July 2021; received in revised form 25 December 2021; accepted 9 May 2022

KEYWORDS
Concentrated winding;
Distributed winding;
Expected load loss;
Fault-tolerant capability;
Magnetic separation;
Open-circuit fault;
Pseudo-concentrated winding;
Physical phase separation;
Reliability analysis;
Six-phase induction machine.

Abstract. Six-phase motors are becoming more popular because of their advantages such as lower torque ripple, better power distribution per phase, higher efficiency, and fault-tolerant capability compared to three-phase ones. This paper presents the fault-tolerant capability analysis of a symmetrical six-phase induction motor equipped with distributed, conventional concentrated, and pseudo-concentrated windings under open-circuit fault scenarios. For further investigation, different load types such as constant-speed, constant-torque, and constant-power are applied to the motor. Two concepts of magnetic and physical phase separations are introduced as factors affecting motor reliability. Analytically, these factors give an insight into how the pseudo-concentrated winding could be a fault-tolerant alternative. Moreover, five parameters including change of output power, power loss, power factor, efficiency, and expected load loss are considered as fault-tolerant capability parameters to evaluate the windings' reliability. The aforementioned parameters are reported using finite element analysis for different fault scenarios and load types. Although the baseline motor dimensions are not optimized for applying the pseudo-concentrated winding, the pseudo-concentrated winding shows promising performance with high fault-tolerant capability.

1. Introduction

In recent years, multi-phase motors have been an attractive option in several applications such as electric vehicle and railway traction, all-electric ships, and more-electric aircraft [1]. Multi-phase motors have several advantages over their three-phase counterparts: splitting the power into multiple phases to reduce the power ratings per phase and improving the distribution of the magneto-motive force in the motor air gap, thereby reducing torque ripples [2]. In addition, the

*. *Corresponding author:*
E-mail address: G.rezazadeh@ut.ac.ir (G. Rezazadeh)

To cite this article:
M., Alemi-Rostami, G., Rezazadeh, F., Tahami, and H.R., Akbari-Resketi, "Fault-tolerant capability analysis of six-phase induction motor with distributed, concentrated, and pseudo-concentrated windings", *Scientia Iranica* (2024), **31**(10), pp. 775-789
DOI: 10.24200/sci.2022.58674.5844

degrees of freedom increase with the number of independent phase variables of the driver, which helps optimize control strategies [3]. One of the most significant advantages of these motors is their high fault-tolerant capability [4], making them suitable for sensitive applications with high reliability requirements. Among the numerous possibilities of multi-phase motors, the six-Phase Induction Motor (6PIM) is one of the most frequently used due to the simplicity of its structure, which is identical to that of a three-phase motor from air gap point of view [5].

Several papers have focused on the structure of the 6PIM in healthy conditions and tried to improve the motor performance parameters [6–9]. Some other papers have studied the post-fault operation of 6PIM under open-phase or short-circuited phase conditions [10–14]. Also, several research studies have focused on the modelling [5,15,16] and control aspects [1,17–19] in post-fault conditions. However, there is no comprehensive fault-tolerant capability analysis for different winding configurations. This paper discusses the fault-tolerant capability of the 6PIM equipped with different winding configurations (such as distributed, concentrated, and pseudo-concentrated windings) under different fault scenarios.

Recently, many valuable published works have focused on the reliability evaluation of electrical machines [20–24]. Various studies on motor reliability have shown that about 30% to 40% of induction motor failures are caused by stator winding faults [25,26]. This fault can arise due to dynamic load conditions or a combination of different stresses acting on the stator winding, such as thermal or electrical stresses [27]. Among the possible faults related to the stator windings, an Open Circuit Fault (OCF) of the stator windings is a common problem [25] and will be discussed here.

In this paper, the performance parameters of the 6PIM equipped with Distributed Winding (DW), Concentrated Winding (CW), and pseudo-CW under different OCF scenarios are examined. In addition, different load types such as constant-speed, constant-torque, and constant-power are employed to study their effects on the motor's reliability. As an analytical approach, two concepts of magnetic and physical phase separations are used, which are closely related to the motor's reliability. These concepts provide insight into how the pseudo-CW could be a fault-tolerant alternative. To more accurately examine the windings' fault-tolerant capability, changes in five parameters (output power, power loss, power factor, efficiency, and expected load loss) are investigated. Finite Element Analysis (FEA) is used to calculate the aforementioned parameters under different fault scenarios and load types. The reliability analysis shows that the pseudo-CW has satisfactory fault-tolerant capability close to the DW and much higher than the CW. It should be noted that the baseline motor is not optimized for applying the pseudo-CW and CW.

Table 1. Baseline motor parameters.

Quantity	Unit	Measured value
External stator diameter	mm	79.5
Internal stator diameter	mm	41.8
Active core length	mm	45.7
Air gap thickness	mm	0.4
Stator slot number	-	24
Stator slot area	mm^2	12.9
Rotor slot number	-	18
Rotor bar area	mm^2	16.8
External end-ring diameter	mm	39.5
Internal end-ring diameter	mm	27
End-ring thickness	mm	7
Inertia coefficient	$kg.m^2$	4.10-4

The paper structure is organized as follows: The configuration of the baseline 6PIM equipped with DW, CW, and pseudo-CW and their performance characteristics are presented in Section 2. The magnetic and physical separation concepts and different possible fault scenarios are explained in Section 3. Motor performance in post-fault conditions is discussed in Section 4. Section 5 presents a comparison between the considered winding layouts from the reliability point of view. Subsequently, a conclusion is presented in Section 6 based on the reported discussions and results.

2. Baseline 6PIM performance

The induction motor with the 24-slot stator and squirrel-cage 18-bar rotor cores is considered as the baseline motor. The main geometrical dimensions of the baseline motor are shown in Table 1. Three different two-pole symmetrical six-phase winding configurations (with a 60° phase shift angle between each phase and its nearest phases) are applied to the baseline 6PIM including: one-layer DW, two-layer conventional CW, and four-layer pseudo-CW (see Figure 1). The performance parameters of the 6PIM equipped with the aforementioned winding layouts are reported in Table 2.

2.1. One-layer DW

The one-layer DW layout is shown in Figure 1(a). By connecting the motor to the power supply (14 V), simulation results from FEA and experimental results are reported in Table 2. According to the simulation results, the no-load current is 1.45 A and the full-load current is 1.82 A. In comparison, the experimental results show 1.41 A and 1.78 A for the no-load and full-

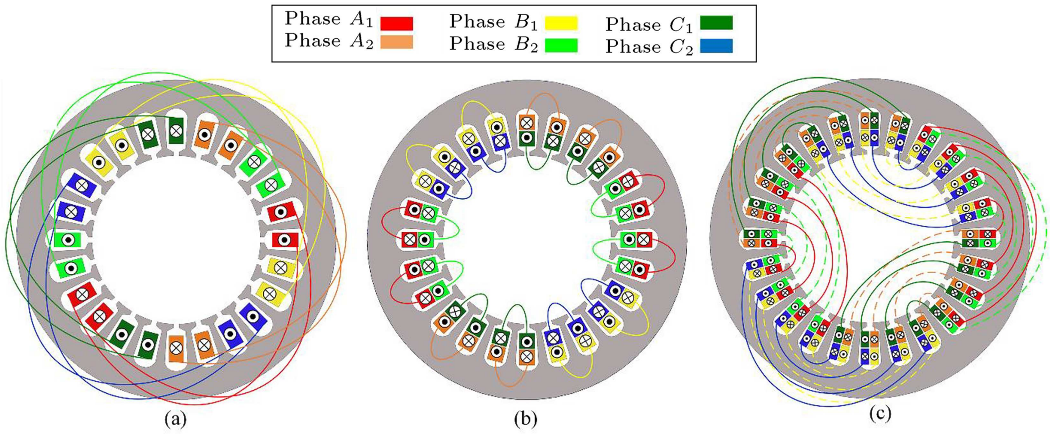

Figure 1. Two-pole winding layouts for the 6PIM: (a) Single-layer DW, (b) two-layer conventional CW, and (c) four-layer pseudo-CW.

Table 2. Performance variables of baseline motor.

Quantity	Unit	DW		CW	Pseudo-CW	
		FEA	Exp [6]	FEA	FEA	Exp [6]
Phase voltage	V	14	14	5.1	10.7	10.7
Turns per slot	-	27	27	28	40	40
Rated current	A	1.82	1.78	1.77	1.78	1.8
No-load current	A	1.45	1.41	1.69	1.62	1.63
Rated speed	rpm	2822	2820	2820	2820	2820
Rated torque	N.m.	0.3	0.3	0.069	0.151	0.16
Power factor	p.u.	0.722	–	0.541	0.651	0.644
Efficiency	%	80.2	–	69.5	60.1	63.6

load currents, respectively. Moreover, FEA simulation results show that the rotor rated speed and torque are 2822 rpm and 0.3 N.m, respectively. It should be noted that the measured values are 2820 rpm and 0.3 N.m, respectively.

2.2. Two-layer CW

The two-layer CW layout is shown in Figure 1(b). As shown in Table 2, the conventional two-layer CW for 6PIM does not perform as well as the other winding layouts because of its low-quality air gap flux density distribution. FEA results show that the conventional two-layer CW has much lower output power compared to the DW at the same rotor speed. The conventional CW, in comparison to DW, has shorter end-winding, which results in less copper usage, smaller resistance, and consequently fewer copper losses [7]. However, the CW efficiency is lower than that of DW because of its low output power value.

2.3. Four-layer pseudo-CW

The pseudo-CW (see Figure 1(c)) layout benefits from the advantages of the CW and has a higher fundamental harmonic amplitude of air gap flux density with lower THD compared to the CW. The performance characteristics of the pseudo-CW are not as good as DW, but they are much higher than those of the CW. Considering the FEA results, the motor has a 1.78 A full-load current, 2820 rpm rated speed, and 0.151 N.m rated torque. In comparison, the experiment has reported 1.8 A, 2820 rpm, and 0.16 N.m, respectively.

3. Magnetic and physical phase separations

3.1. Physical phase separation

The motor hot spot is usually placed in the stator slots where the major heat source (conductive loss) cannot be easily dissipated, leading to damage to the insulation winding [28]. Stator winding faults are generally related to insulation failure, starting as undetected turn-turn faults and eventually growing into phase-phase faults [25]. One winding feature that can prevent the initiation of phase-phase faults is the physical phase separation between different phases. The most complete type of physical separation occurs when only one coil is placed in each slot (using single-layer configuration) and no overlapping between different phases occurs in the end winding. For example, in a single-layer DW configuration, there is overlapping in the end-winding region. Therefore, among the different winding types, the single-layer CW (winding on tooth) has the most physical separation between different phases.

As shown in Figure 1(a), in the end-winding region of the DW, phase A_1 is in contact with all phases except phase B_2. This is because, in the short-pitch DW configuration, each phase is not in contact with its opposite phase. Conversely, in the conventional full-pitch DW, each phase is in contact with all the other phases, resulting in a bulky end-winding. However, the heat produced by winding conductive loss could be trapped in this bulky end-winding, causing a heat transferring problem. From an analytical point of view, the physical phase separation of the DW configuration is not acceptable.

In the CW configuration, each phase is in contact with two other phases in the slots because of its two-layer configuration, and no winding overlap is seen in the end-winding part. In the considered four-layer pseudo-CW, each phase is in contact with three other phases in the stator slots, and no overlap between different phases occurs in the end winding part [6].

It should be noted that the baseline 6PIM is not optimized for applying pseudo-CW and its dimensions were designed for DW application. In [6], where the performance parameters of 6PIMs in healthy condition are reported, the four-layer pseudo-CW is proposed for the first time to achieve higher performance parameters compared to CW. Since only the performance results of the four-layer pseudo-CW were available, they were eventually compared with the single-layer DW and the two-layer CW. Considering the physical separation results, the pseudo-CW exhibits a more satisfying condition than DW.

3.2. Magnetic separation

Beside the physical phase separation, magnetic separation between different phases is an important parameter to enhance the fault tolerant capability [29]. Without magnetic isolation, fault in one phase can induce voltages in other phases. Thus, the motor should be designed with minimal mutual coupling between different phases. In other words, a zero mutual inductance between phases and high self-inductance for each phase are the most suitable magnetic characteristics for the motor considering the reliability aspect, because these features prevent spreading the fault from one phase to the another magnetically.

The ratio of the mutual inductance between the different phases to the self-inductance of the phase is considered as an index to measure a motor's fault tolerant capability. This ratio should be close to zero in an ideal condition where the phases are fully separated magnetically [30]. It should be noted that this ratio is not a novel parameter to investigate the fault tolerant capability, as its concept is reported in [30] and its related calculations are presented in [31]. The inductance ratio for the fault-tolerant capability between phase x and phase y is:

$$IRFT_{xy} = \frac{L_{xy}}{L_{xx}}. \tag{1}$$

Assuming that the air gap length is a constant value for all spatial angles (φ), the mutual inductance between phases x and y would be [31]:

$$L_{xy} = \frac{\psi_{xy}}{i_x} = \frac{\mu_0 Rl}{g} \int_0^{2\pi} N_x(\varphi).TF_y(\varphi)d\varphi. \tag{2}$$

In Eq. (2), ψ_{xy} is the mutual flux linkage between phases x and y, and TF_x is the turn function of the phase x. The self-inductance of phase x is [31]:

$$L_{xx} = \frac{\mu_0 Rl}{g} \int_0^{2\pi} N_x(\varphi).TF_x(\varphi)d\varphi. \tag{3}$$

For the pseudo-CW, this ratio is equal to 0.227 between phase A_1 and other phases except for phase B_2. Phase B_2 is a redundant phase of phase A_1 and has a similar configuration to phase A_1 with opposite direction of current flow, so it is obvious that this phase has a strong magnetic coupling to phase A_1 ($IRFT_{A_1B_2} = 1$). According to the results, the pseudo-CW ($IRFT_{Pseudo-CW} = 0.227$) has more separated phases magnetically than DW ($IRFT_{DW} = 0.423$) and less than CW ($IRFT_{CW} = 0$). Therefore, even if the baseline motor dimensions are not optimized for the pseudo-CW, the results are satisfying. The FEA results for the phases inductance matrix are reported in Table 3. As can be seen, the FEA results completely validate the accuracy of the obtained analytical results considering phase-to-phase inductance, phase self-inductances, and $IRFT$ values. It should be noted that the slight difference between the analytical and FEA results arises from the fact that FEA takes more magnetic aspects into account, such as slotting effect, core nonlinear magnetic behavior, and coil leg placement in slot layers.

4. Faulty and healthy conditions report using FEA

The six-phase motor has the ability to operate under OCF conditions, where up to 3 phases are lost. As shown in Figure 2, five different OCF types, which could occur in the six-phase motor and still allow the motor to continue producing torque, are one-Phase (IPh), Adjacent double-Phase (A2Ph), Non-Adjacent double-Phase (NA2Ph), Adjacent triple-Phase (A3Ph), and Non-Adjacent triple-Phase (NA3Ph) faults. Table 4 presents the fault scenarios considering seven possible open-circuit faults. These scenarios were studied on the 6PIM equipped with DW, CW, and pseudo-CW. It should be noted that each explained fault scenario

Table 3. FEA results for phase-to-phase inductances: (a) Distributed Winding (DW), (b) conventional Concentrated Winding (CW), and (c) pseudo-CW.

(a) Distributed winding

Phases	Phase A_1	Phase A_2	Phase B_1	Phase B_2	Phase C_1	Phase C_2
Phase A_1	1	0.4285	0.4285	0.8931	0.4285	0.4285
Phase A_2	0.4285	1	0.4285	0.4285	0.8931	0.4285
Phase B_1	0.4285	0.4285	1	0.4285	0.4285	0.8931
Phase B_2	0.8931	0.4285	0.4285	1	0.4285	0.4285
Phase C_1	0.4285	0.8931	0.4285	0.4285	1	0.4285
Phase C_2	0.4285	0.4285	0.8931	0.4285	0.4285	1

(b) Conventional concentrated winding

Phases	Phase A_1	Phase A_2	Phase B_1	Phase B_2	Phase C_1	Phase C_2
Phase A_1	1	0.0169	0.0169	0.0341	0.0169	0.0169
Phase A_2	0.0169	1	0.0169	0.0169	0.0341	0.0169
Phase B_1	0.0169	0.0169	1	0.0169	0.0169	0.0341
Phase B_2	0.0341	0.0169	0.0169	1	0.0169	0.0169
Phase C_1	0.0169	0.0341	0.0169	0.0169	1	0.0169
Phase C_2	0.0169	0.0169	0.0341	0.0169	0.0169	1

(c) Pseudo-CW

Phases	Phase A_1	Phase A_2	Phase B_1	Phase B_2	Phase C_1	Phase C_2
Phase A_1	1	0.2331	0.2331	0.9659	0.2331	0.2331
Phase A_2	0.2331	1	0.2331	0.2331	0.9659	0.2331
Phase B_1	0.2331	0.2331	1	0.2331	0.2331	0.9659
Phase B_2	0.9659	0.2331	0.2331	1	0.2331	0.2331
Phase C_1	0.2331	0.9659	0.2331	0.2331	1	0.2331
Phase C_2	0.2331	0.2331	0.9659	0.2331	0.2331	1

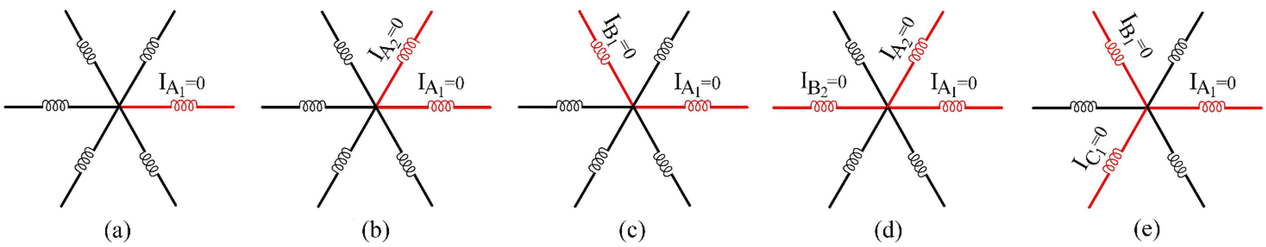

Figure 2. Open-circuit faults in phase windings of 6PIM: (a) 1Ph, (b) A2Ph, (c) NA2Ph, (d) A3Ph, and (e) NA3Ph.

occurs with six different combinations involving different phases involved.

The motor is simulated in healthy and faulty conditions using the FEA. The FEA results are obtained by using a time-transient simulation in 2D Ansys Maxwell software. The flux density distribution of the 6PIM equipped with DW under healthy and two-phase fault condition are shown in Figure 3. Similarly, the flux density distributions of the 6PIM equipped with CW and pseudo-CW are shown in Figures 4 and 5, respectively. As can be seen, when the OCF occurs, the flux density amplitude is reduced, especially in the stator and rotor teeth. This reduction is due to the absence of some of the flux producing sources (resulting from the occurrence of the OCF), as the phase currents are the source of producing flux in the stator and rotor magnetic paths. In Figure 6, the phase current under a 2A OCF scenario is shown for different winding types. The presence of current harmonics is evident and results in higher output torque ripple. The FEA simulation results of the 6PIM equipped with DW, CW, and pseudo-CW under different scenarios are reported in Tables 5 to 7. The results were obtained using three different load types: constant-speed, constant-torque, and constant-power, to consider the effects of load type on the motor's fault-tolerant capability.

The obtained results show that when an OCF

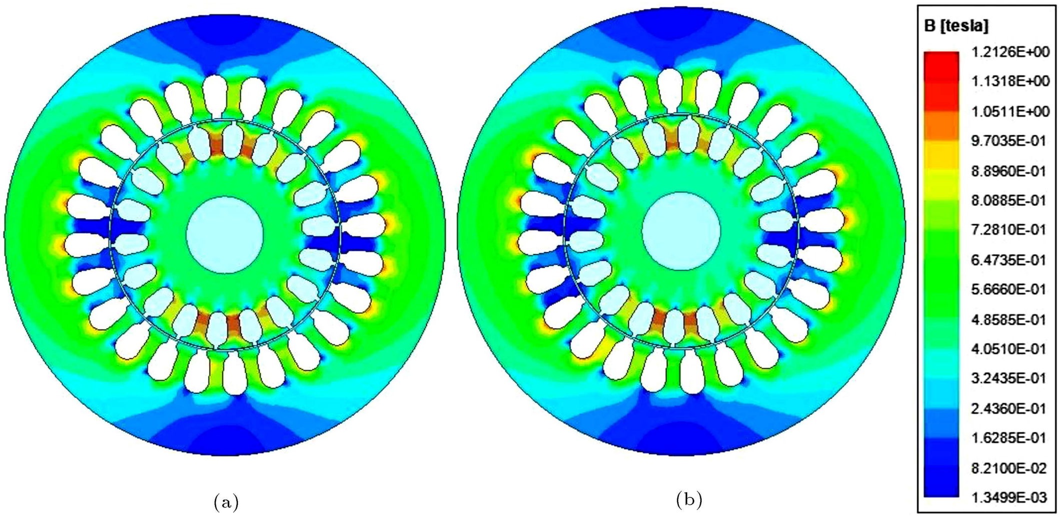

Figure 3. FEA results for flux density distribution of DW: (a) Healthy condition and (b) 2A OCF scenario.

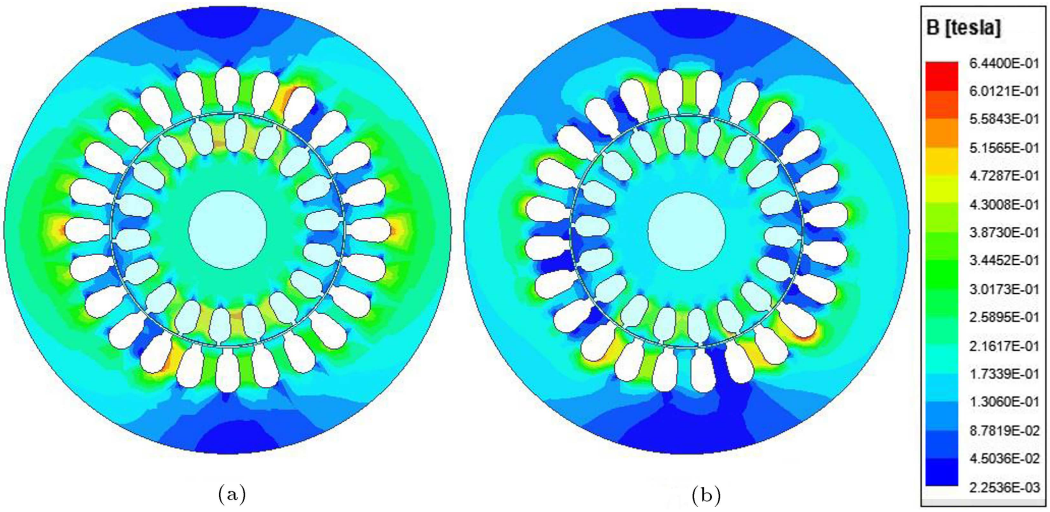

Figure 4. FEA results for flux density distribution of CW: (a) Healthy condition and (b) 2A OCF scenario.

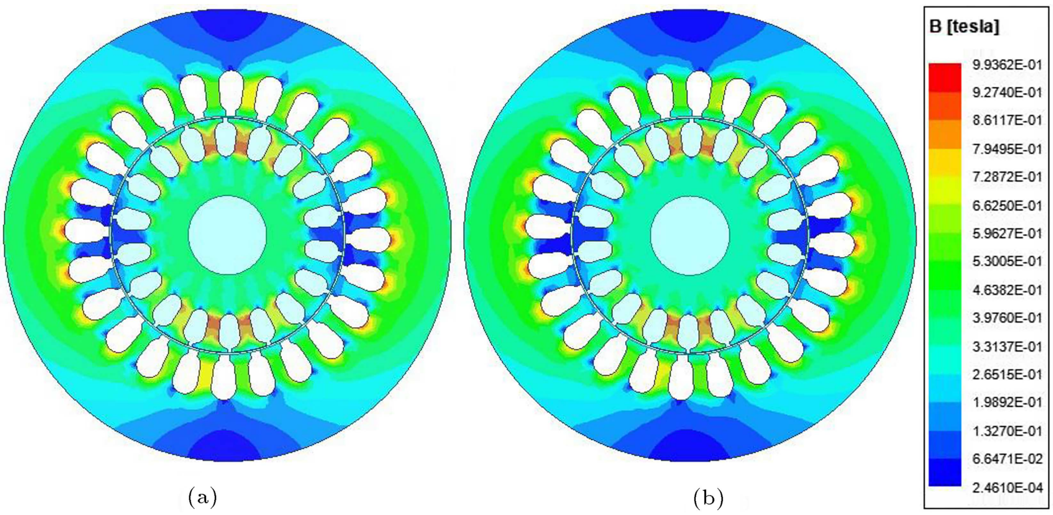

Figure 5. FEA results for flux density distribution of pseudo-CW: (a) Healthy condition and (b) 2A OCF scenario.

Table 4. Different fault scenarios for symmetrical six-phase induction motor.

OCF		Scenarios	Phase fault
Number of OCFs	**Faults**		
0 OCF	0Ph	0A	–
1 OCF	1Ph	1A	A_1
2 OCFs	A2Ph	2A	A_1-A_2
	NA2Ph	2B	A_1-B_1
	NA2Ph	2C	A_1-B_2
3 OCFs	A3Ph	3A	A_1-A_2-B_1
	NA3Ph	3B	A_1-A_2-B_2
	NA3Ph	3C	A_1-B_1-C_1

occurs, the current in the adjacent phase increases to compensate for the reduced MMF. In other words, if one or more phases are lost, the current in healthy phases increases to maintain the power of the motor. In this situation, the power losses of the remaining phases increase, potentially causing damage to the windings. For this reason, a power derating factor is required to keep the windings safe. It should be noted that as the number of phase faults increases, the derating factor also increases. Therefore, spreading the fault from one phase to another has a great impact on the derating factor in the post-fault condition. Therefore, increased physical and magnetic separation between phases could help reduce the amount of load loss in the post-fault condition. As can be seen in Table 4, during the 1 A scenario, the current flow through the stator increases by approximately 1.2 times in phases A_2 and B_1, 1.3 times in phase B_2, and 1.14 times in phases C_1 and C_2 for the 6PIM equipped with DW using a constant-speed load compared to the healthy condition.

It should be noted that the conventional CW (applied to the baseline 6PIM) does not exhibit proper performance parameters even in healthy conditions. Moreover, the winding performance gets worse in post-fault conditions, especially when constant-power or constant-torque are applied. Consequently, the motor cannot produce enough power to rotate the load. To ensure reliable results for comparison and avoid unjustified performance results, the FEA results for

Table 5. FEA results for performance of 6PIM equipped with DW: (a) Constant-speed, (b) constant-torque, and (c) constant-power.

Scenarios	Parameter							Torque		Speed	Copper loss	P_{LL}	Power factor	P_{out}	Efficiency
	Vph	I_{A1}	I_{A2}	I_{B1}	I_{B2}	I_{C1}	I_{C2}	Full load torque	Torque ripple						
(a) Constant-speed															
0A	14	1.76	1.76	1.76	1.76	1.76	1.76	0.3	26%	2822	18.6	0.00	0.81	88.66	74%
1A	14	0	2.12	2.14	2.24	2	2.02	0.29	56%	2822	22.2	2.96	0.73	85.70	73%
2A	14	0	0	2.47	2.68	2.61	2.29	0.25	70%	2822	25.3	8.66	0.67	80.00	69%
2B	14	0	2.36	0	2.67	2.41	2.58	0.26	74%	2822	25.2	9.26	0.67	79.40	68%
2C	14	0	2.51	2.49	0	2.54	2.51	0.26	120%	2822	25.3	11.66	0.67	77.00	67%
3A	14	0	0	0	3.28	3.24	3.05	0.238	30%	2822	30.6	18.66	0.59	70.00	63%
3B	14	0	0	3.04	0	3.36	3.01	0.232	145%	2822	29.6	19.16	0.60	69.50	62%
3C	14	0	3.13	0	3.16	0	3.14	0.231	26%	2822	29.6	19.66	0.60	69.00	62%
(b) Constant-torque															
0A	14	1.76	1.76	1.76	1.76	1.76	1.76	0.3	25%	2822	18.6	0.00	0.81	88.66	74%
1A	14	0	2.12	2.1	2.24	2.1	2.02	0.3	60%	2812	22.4	0.31	0.76	88.34	71%
2A	14	0	0	2.67	2.82	2.8	2.46	0.3	64%	2790	29.0	1.01	0.73	87.65	65%
2B	14	0	2.54	0	2.82	2.6	2.75	0.3	68%	2791	28.7	0.97	0.74	87.68	64%
2C	14	0	2.68	2.67	0	2.74	2.65	0.3	112%	2787	28.8	1.10	0.73	87.56	65%
3A	14	0	0	0	3.74	3.72	3.52	0.3	30%	2754	40.2	2.14	0.65	86.52	61%
3B	14	0	0	3.67	0	4.1	3.61	0.3	134%	2730	43.3	2.89	0.71	85.77	54%
3C	14	0	3.7	0	3.74	0	3.72	0.3	22%	2745	41.5	2.42	0.66	86.24	59%
(c) Constant-power															
0A	14	1.79	1.79	1.79	1.79	1.79	1.79	0.3	26%	2822	19	0.00	0.80	88.66	74%
1A	14	0	2.12	2.12	2.25	2.08	2.01	0.3	56%	2813	22	0.28	0.77	88.37	71%
2A	14	0	0	2.62	2.81	2.81	2.46	0.302	68%	2792	29	0.36	0.71	88.30	68%
2B	14	0	2.51	0	2.89	2.65	2.76	0.305	65%	2757	29	0.60	0.70	88.06	68%
2C	14	0	2.81	2.72	0	2.77	2.7	0.308	120%	2747	30	0.05	0.72	88.60	65%
3A	14	0	0	0	3.87	3.86	3.65	0.311	29%	2705	43	0.56	0.66	88.10	60%
3B	14	0	0	3.8	0	4.33	3.7	0.311	128%	2670	47	1.70	0.67	86.96	55%
3C	14	0	3.82	0	3.82	0	3.85	0.312	24%	2670	44	1.70	0.65	86.96	59%

Table 6. FEA results for performance of 6PIM equipped CW: Constant-speed.

Constant-speed															
Scenarios	Parameter							Torque		Speed	Copper loss	P_{LL}	Power factor	P_{out}	Efficiency
	Vph	I_{A1}	I_{A2}	I_{B1}	I_{B2}	I_{C1}	I_{C2}	Full load torque	Torque ripple						
0A	5.1	1.77	1.77	1.77	1.77	1.77	1.77	0.069	110%	2820	9.40	0.00	0.63	20.38	61%
1A	5.1	0	2.4	1.85	1.26	2.41	1.88	0.064	180%	2820	10.06	1.48	0.60	18.90	58%
2A	5.1	0	0	2.5	1.21	1.68	2.58	0.034	217%	2820	8.26	10.34	0.49	10.04	46%
2B	5.1	0	2.58	0	1.7	2.44	1.41	0.036	208%	2820	9.92	9.75	0.50	10.63	44%
2C	5.1	0	2.9	2.15	0	2.88	2.14	0.041	280%	2820	12.95	0.30	0.52	20.08	42%
3A	5.1	0	0	0	1.86	1.56	1.99	0.016	600%	2820	6.27	15.65	0.40	4.72	33%
3B	5.1	0	0	2.7	0	1.91	2.68	0.014	950%	2820	9.06	16.24	0.44	4.13	25%
3C	5.1	0	1.99	0	2	0	1.98	0.013	760%	2820	8.70	16.54	0.38	3.84	24%

Table 7. FEA results for performance of 6PIM equipped pseudo-CW: (a) Constant-speed, (b) constant-torque, and (c) constant-power.

(a) Constant-speed															
Scenarios	Parameter							Torque		Speed	Copper loss	P_{LL}	Power factor	P_{out}	Efficiency
	Vph	I_{A1}	I_{A2}	I_{B1}	I_{B2}	I_{C1}	I_{C2}	Full load torque	Torque ripple						
0A	10.7	1.78	1.78	1.78	1.78	1.78	1.78	0.151	30%	2820	19	0.00	0.62	44.59	63%
1A	10.7	0	2.01	1.80	2.29	2.03	1.80	0.148	80%	2820	20	0.98	0.61	43.61	61%
2A	10.7	0	0	2.16	2.41	2.71	2.19	0.135	80%	2820	23	4.67	0.56	39.93	57%
2B	10.7	0	2.13	0	2.69	2.20	2.39	0.133	78%	2820	22	5.28	0.56	39.31	57%
2C	10.7	0	2.63	1.94	0	2.59	2.00	0.128	150%	2820	21	6.82	0.55	37.78	57%
3A	10.7	0	0	0	2.94	2.97	3.00	0.120	28%	2820	26	9.27	0.51	35.32	51%
3B	10.7	0	0	2.96	0	3.12	2.93	0.119	148%	2820	30	9.58	0.50	35.01	48%
3C	10.7	0	2.96	0	2.99	0	3.00	0.121	27%	2820	27	8.97	0.52	35.63	51%

(b) Constant-torque															
Scenarios	Parameter							Torque		Speed	Copper loss	P_{LL}	Power factor	P_{out}	Efficiency
	Vph	I_{A1}	I_{A2}	I_{B1}	I_{B2}	I_{C1}	I_{C2}	Full load torque	Torque ripple						
0A	10.7	1.78	1.78	1.78	1.78	1.78	1.78	0.151	30%	2820	19	0.00	0.62	44.59	63%
1A	10.7	0	2.06	1.84	2.32	2.10	1.82	0.151	80%	2811	21	0.14	0.61	44.46	61%
2A	10.7	0	0	2.31	2.57	2.89	2.32	0.151	80%	2775	26	0.71	0.58	43.88	57%
2B	10.7	0	2.31	0	2.89	2.29	2.57	0.151	78%	2783	25	0.58	0.58	44.01	57%
2C	10.7	0	3.02	2.25	0	3.01	2.28	0.151	150%	2735	28	1.34	0.56	43.25	55%
3A	10.7	0	0	0	3.32	3.33	3.33	0.151	28%	2723	33	1.54	0.55	43.06	51%
3B	10.7	0	0	3.52	0	3.71	3.47	0.151	141%	2709	38	1.76	0.55	42.83	48%
3C	10.7	0	3.32	0	3.36	0	3.37	0.151	27%	2720	34	1.58	0.55	43.01	51%

(c) Constant-power															
Scenarios	Parameter							Torque		Speed	Copper loss	P_{LL}	Power factor	P_{out}	Efficiency
	Vph	I_{A1}	I_{A2}	I_{B1}	I_{B2}	I_{C1}	I_{C2}	Full load torque	Torque ripple						
0A	10.7	1.78	1.78	1.78	1.78	1.78	1.78	0.151	26%	2820	19	0.00	0.62	44.59	63%
1A	10.7	0	2.05	1.84	2.32	2.06	1.81	0.151	64%	2802	21	0.28	0.61	44.31	61%
2A	10.7	0	0	2.33	2.57	2.86	2.34	0.153	70%	2760	26	0.37	0.58	44.22	57%
2B	10.7	0	2.34	0	2.90	2.33	2.57	0.153	70%	2760	26	0.37	0.58	44.22	57%
2C	10.7	0	3.19	2.38	0	3.19	2.40	0.16	138%	2650	32	0.19	0.57	44.40	53%
3A	10.7	0	0	0	3.48	3.46	3.48	0.156	24%	2700	36	0.48	0.56	44.11	50%
3B	10.7	0	0	3.71	0	3.90	3.58	0.155	136%	2690	42	0.93	0.55	43.66	47%
3C	10.7	0	3.47	0	3.52	0	3.50	0.155	22%	2675	37	0.89	0.55	43.70	50%

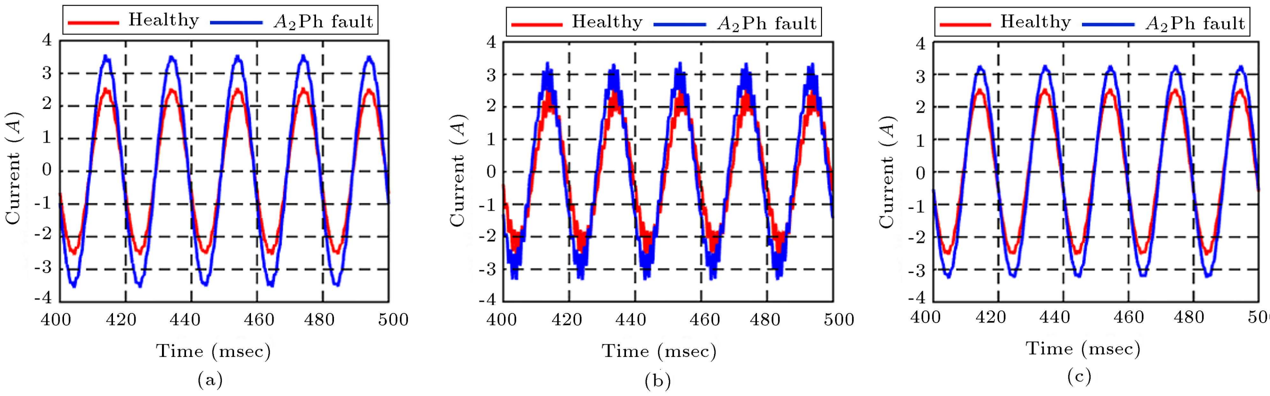

Figure 6. Phase current waveforms in healthy and faulty conditions: (a) DW, (b) CW, and (c) pseudo-CW.

the performance of the 6PIM equipped with CW are not reported in post-fault conditions when constant-power and constant-torque load types are applied to the motor. This decision is made because the motor cannot operate properly under these conditions.

5. Fault tolerant analysis

5.1. Reliability

After presenting the motor performance parameters in post-fault conditions, these parameters could be used in a reliability analysis to investigate the fault-tolerant capability of the 6PIM equipped with DW, CW, and pseudo-CW. To use this analysis method, first, some fundamental aspects of reliability analysis should be explained here. Reliability is the probability of performing adequately to achieve the desired aim of the system in a specified time [32].

One of the useful reliability indices to evaluate the motor fault-tolerant capability is the Expected Load Loss (ELL), which indicates the expected amount of load that cannot be supplied in a post-fault condition considering the fault occurrence probability [33]. The ELL can be calculated as [34]:

$$ELL = \sum_{i=1}^{n} (PLL) \times P_{LL}. \quad (4)$$

As can be seen, the ELL value depends on the Probability of Load Loss (PLL) and the load loss amount (P_{LL}). Before proceeding to the probability part of the reliability analysis (PLL calculation), it is necessary to express the utilized assumptions for the reliability analysis. To simplify the reliability analysis procedure, some assumptions are used as follows:

1. The probability of losing each phase is equal to $Q(t)$, which is a function of time;
2. The fault occurrence in each phase is independent of the operation conditions of other phases. In other words, fault occurrence in phases is an independent probability event.

Now, it is necessary to calculate $Q(t)$ for fault occurrence in each phase. Considering the reliability concept, the probability of a component (winding phase) surviving for a time t with a constant failure rate of λ is [22]:

$$P(t) = e^{-\lambda t}. \quad (5)$$

Therefore, the probability of fault occurrence in each phase can be described as:

$$Q(t) = 1 - P(t) = 1 - e^{-\lambda t}. \quad (6)$$

An example for calculating the (P_{LL}) for the OCF scenario where A_1 and B_1 are the faulty phases could clarify how P_{LL} value is related to $P(t)$ and $Q(t)$. In this scenario, four components are up and two components are down, so the probability is:

$$P(faulty\ phases : A_1\ \&\ B_1) = P^4(t)Q^2(t)$$
$$= e^{-4\lambda t}(1 - e^{-\lambda t})^2. \quad (7)$$

It should be noted that there are many OCF scenarios for each case study; therefore, the ELL formula for each case study (6PIM with each winding configuration) is too long. Thus, the obtained ELL equations of the case studies are not reported in this paper for the sake of brevity.

The failure rate of the 6PIM phase winding is equal to 15×10^{-8} [22]. Using the presented equations and the utilized failure rate, the ELL values for the 6PIM equipped with different winding configurations are calculated after one million hours and will be discussed in the next section. It should be noted that for ELL calculation, the FEA simulation results are used for the amount of load loss.

5.2. Results and discussion

The effect of OCF occurrence on five performance parameters such as output power, power loss, power factor, efficiency, and expected load loss are investigated to evaluate the windings' reliability. These

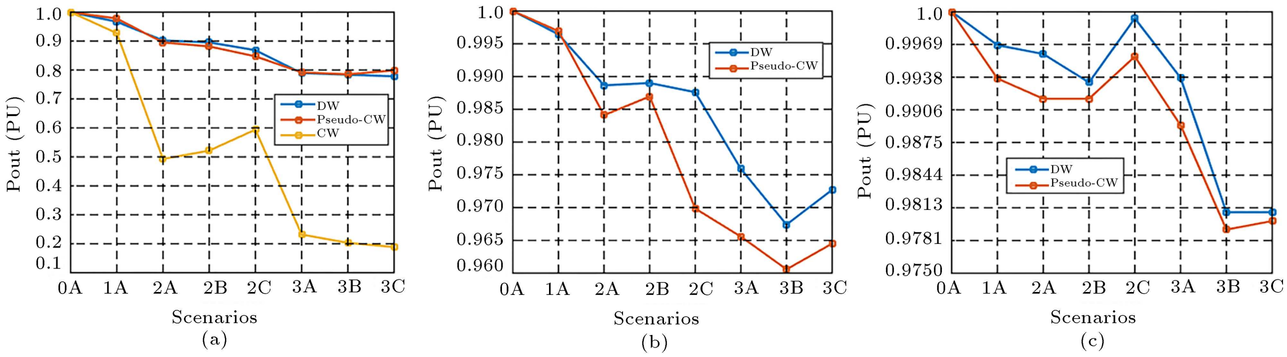

Figure 7. Output power of 6PIM under different fault scenarios: (a) Constant-speed, (b) constant-torque, and (c) constant-power load types.

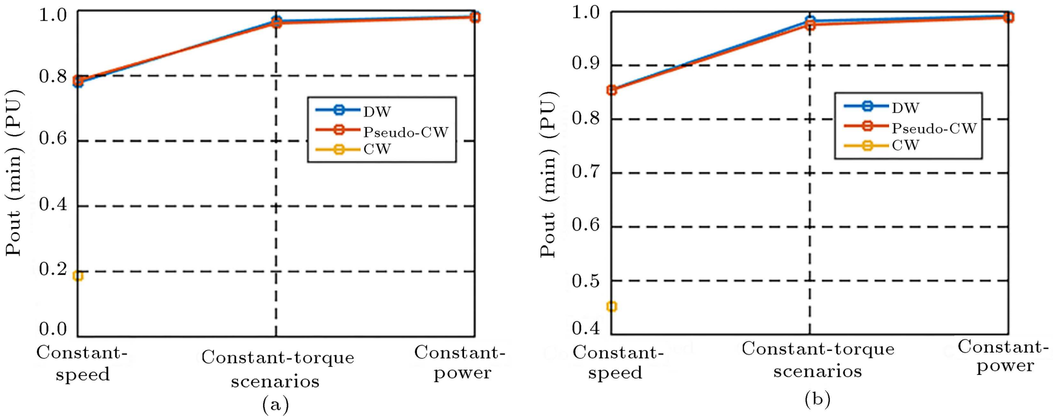

Figure 8. FEA results for (a) Minimum and (b) Average normalized output powers of 6PIMs with DW, CW, and pseudo-CW.

parameters are carefully studied using the FEA results as follows:

(1) Output power: Figure 7 shows the output power of the 6PIM equipped with DW, CW, and pseudo-CW in different fault scenarios with different load types. In constant-torque and constant-power load types, the change in output power is negligible because the loads demand almost constant output power. Considering this fact, the best load type to study the effect of fault occurrence on output power is the constant-speed one. In constant-speed load, the normalized output powers of the 6PIM equipped with pseudo-CW are very close to those of the 6PIM with DW in different scenarios. Even in the 1A and 3C scenarios, the output power reduction of the pseudo-CW is less than that of the DW.

However, the output power variation of the CW in different OCF scenarios shows an unacceptable fault-tolerant capability for the CW, even if the CW has the highest phase separation compared to the DW and pseudo-CW. The main reason for this is the fact that even in a healthy condition, the CW does not have proper performance parameters and is not a suitable winding configuration for IM applications. On the other hand, the pseudo-CW exhibits satisfactory fault-tolerant capability considering the output power reduction compared to the DW.

To investigate the windings' output power in faulty conditions even more, Figure 8 shows the minimum and average output power for the 6PIM equipped with DW, CW, and pseudo-CW when different load types are applied to the motor. As can be seen once more, the pseudo-CW provides similar minimum and average output power close to those of the DW in post-fault conditions.

(2) Power loss: Figure 9 shows the normalized power loss of the 6PIM equipped with the considered winding layouts. Considering these results, it is clear that the motor power loss increases after fault occurrence as expected. However, the pseudo-CW has higher power loss growth than the CW, and fortunately lower than that of the DW. Therefore, the pseudo-CW has better fault-tolerant capability compared to the DW, considering the power loss growth factor.

For further investigation, Figure 10 shows the minimum and average power loss for the 6PIM equipped with DW, CW, and pseudo-CW when dif-

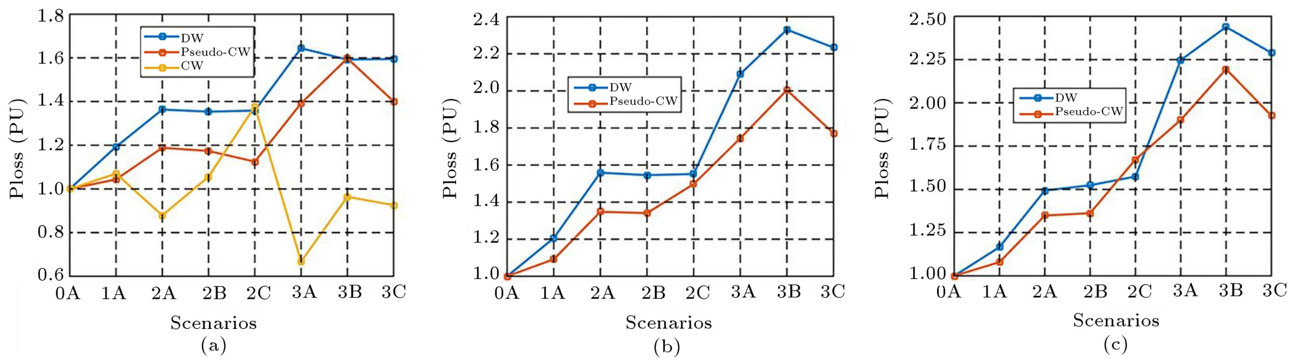

Figure 9. Power loss of 6PIM under different fault scenarios: (a) Constant-speed (b) Constant-torque (c) Constant-power load types.

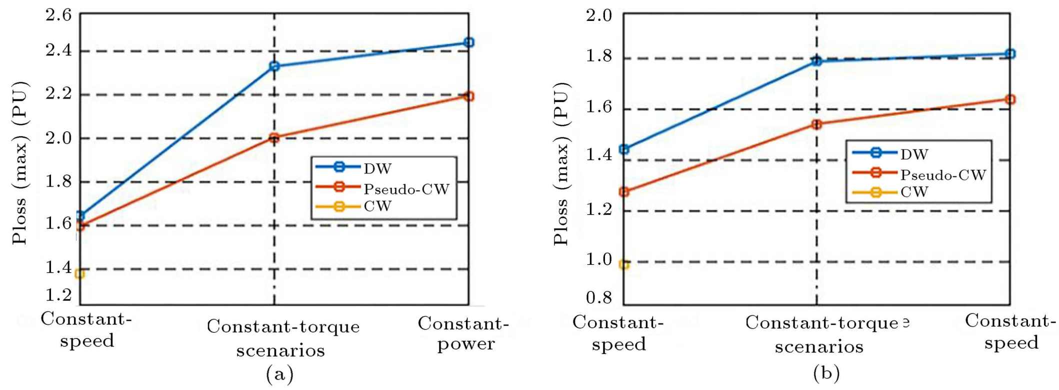

Figure 10. FEA results for (a) Minimum and (b) Average power losses of 6PIMs with DW, CW, and pseudo-CW.

ferent load types are applied to the motor. Clearly, the power loss growth when using the pseudo-CW is lower than with the DW.

(3) Efficiency: As mentioned multiple times, the baseline 6PIM laminations are designed for the application of DW, thus, the DW has the best efficiency in healthy conditions. By reporting the absolute value of the efficiency for different winding configurations, the DW will have the highest efficiency values in every fault scenario because of its superior performance in the designed laminations. However, the aim of this paper is only to discuss the effect of OCF occurrence on different windings to evaluate their fault-tolerant capability. Therefore, instead of reporting the absolute value of the windings' efficiency, their efficiency regulation value compared to their healthy condition will be reported as follows:

$$\eta\, regulation(\%) = \frac{\eta_{healthy} - \eta_{mutual}}{\eta_{healthy}} \times 100. \quad (8)$$

This way, the change in efficiency value caused by fault occurrence can be easily observed. Figure 11 shows the efficiency regulation for the 6PIM equipped with the considered winding layouts. As can be seen, the pseudo-CW has similar changes in efficiency value as the DW. However, the CW has unacceptable behavior compared to the other winding layouts. It can be stated that in terms of the efficiency parameter, the pseudo-CW and DW are the layouts with satisfying fault-tolerant capability.

(4) Power factor: The changes in power factor are investigated using the same scenario as that employed for the efficiency. In other words, the power factor regulation is chosen to be studied instead of the actual absolute value of the power factor:

$$PF\, regulation(\%) = \frac{PF_{healthy} - PF_{mutual}}{PF_{healthy}} \times 100. \quad (9)$$

As shown in Figure 12, the pseudo-CW has the highest fault-tolerant capability compared to the CW and DW, considering the reported power factor variation in different load types and OCF scenarios.

(5) Expected load loss: Using the reliability analysis presented in the previous section, the expected load loss values for the 6PIM equipped with DW, pseudo-CW, and CW are calculated across different load types. The obtained ELL equations are functions of time with long length; therefore, to make it possible to compare the windings' ELL values, the ELL values are reported after one million hours and using the phase failure rate of 15 ×

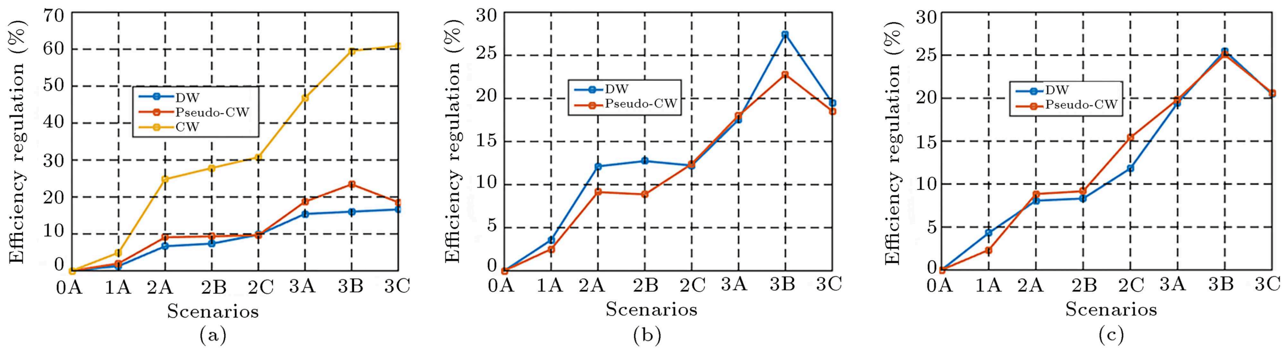

Figure 11. Efficiency of 6PIM under different fault scenarios: (a) Constant-speed (b) Constant-torque (c) Constant-power load types.

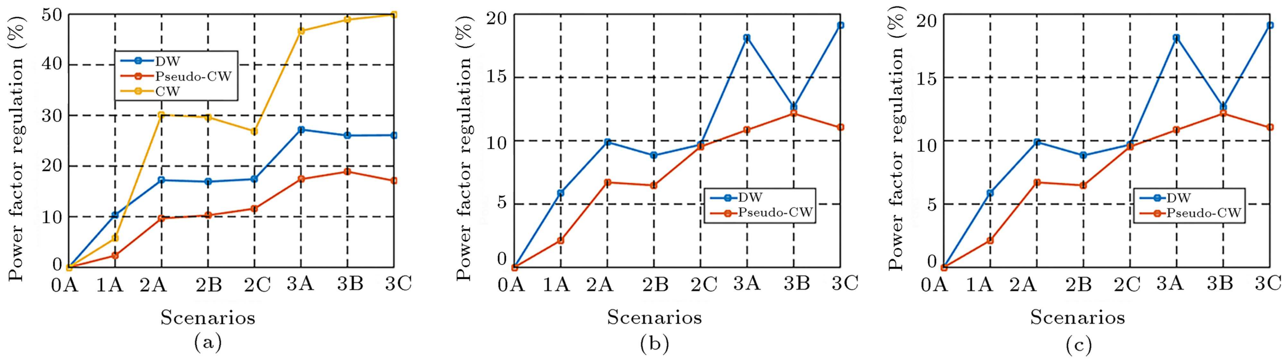

Figure 12. Power factor of 6PIM under different fault scenarios: (a) Constant-speed (b) Constant-torque (c) Constant-power load types.

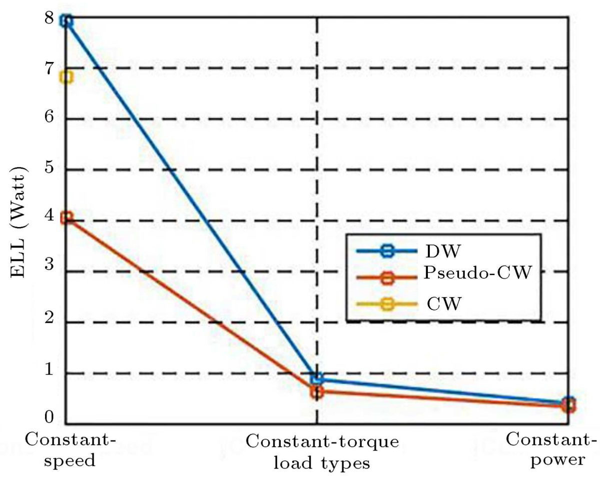

Figure 13. ELL of 6PIM under different load conditions.

10^{-8}. The calculated ELL results are reported in Figure 13. As can be seen, the pseudo-CW has approximately 46%, 31%, and 8% lower ELL values compared to the DW in constant-speed, constant-torque, and constant-power load types, respectively. In addition, it has a 37% lower ELL value compared to the CW in constant-speed load type. Therefore, considering all five reliability parameters, especially the ELL, it can be concluded that the pseudo-CW has the highest fault-tolerant capability compared to the CW and DW. It should be noted that the fault-tolerant capability of the pseudo-CW could be enhanced even more with a proper redesign of the 6PIM dimensions [10].

6. Conclusion

This paper presented a fault-tolerant capability analysis of the six-Phase Induction Motor (6PIM) equipped with Distributed Winding (DW), Concentrated Winding (CW), and pseudo-CW under various Open Circuit Fault (OCF) scenarios (losing up to three phases) and different load types (constant-speed, constant-power, and constant-torque). Two concepts of magnetic and physical phase separations were considered, which impact the motor's reliability. The results showed that the CW has the best and DW the worst phase separation, both magnetically and physically.

Continuing the analysis, five parameters-efficiency, power factor, output power, power loss, and expected load loss-were studied in post-fault conditions to monitor the windings' behavior after fault occurrence. Investigating these parameters showed that the pseudo-CW has higher fault-tolerant capability compared to the DW and CW, with much lower (from 8% to 53%) ELL values across different load types. It should be mentioned that the pseudo-CW was applied to the 6PIM laminations designed for DW application; therefore, by designing a completely new motor compatible with pseudo-CW features, motor performance and, consequently, its fault-tolerant capability could be enhanced.

It can be concluded that although the CW has the highest phase separation, it lacks acceptable fault-tolerant capability compared to DW and pseudo-CW. The main reason is that even in healthy conditions, the CW does not have proper performance parameters, and it is not a suitable winding configuration for 6PIM application.

References

1. Baneira, F., Doval-Gandoy, J., Yepes, A.G., et al. "Comparison of postfault control strategies in terms of converter losses for dual three-phase machines", *IEEE Energy Conversion Congress and Exposition (ECCE)*, pp. 3612–3619 (2017). DOI: 10.1109/ECCE.2017.8096641

2. Abdel-Khalik, A.S., Hamad, M.S., Massoud A.M., et al. "Postfault operation of a nine-phase six-terminal induction machine under single open-line fault", *IEEE Transactions on Industrial Electronics*, **65**(2), pp. 1084–1096 (2017). DOI: 10.1109/TIE.2017.2733471

3. Salem, A. and Narimani, M. "A review on multiphase drives for automotive traction applications", *IEEE Transactions on Transportation Electrification*, **5**(4), pp. 1329–1348 (2019). DOI: 10.1109/TTE.2019.2956355

4. Baneira, F., Yepes, A.G., López, Ó., et al. "Estimation method of stator winding temperature for dual three-phase machines based on dc-signal injection", *IEEE Transactions on Power Electronics*, **31**(7), pp. 5141–5148 (2015). DOI: 10.1109/TPEL.2015.2479410

5. Kianinezhad, R., Nahid-Mobarakeh, B., Baghli, L., et al. "Modeling and control of six-phase symmetrical induction machine under fault condition due to open phases", *IEEE Transactions on Industrial Electronics*, **55**(5), pp. 1966–1977 (2008). DOI: 10.1109/TIE.2008.918479

6. Rezazadeh, G., Tahami, F., Capolino, G.A., et al. "Improvement of concentrated winding layouts for six-phase squirrel cage induction motors", *IEEE Transactions on Energy Conversion*, **35**(4), pp. 1727–1735 (2020). DOI: 10.1109/TEC.2020.2995433

7. Rezazadeh, G., Vaschetto, S., Tahami, F., et al. "Analysis of six-phase induction motor with distributed and concentrated windings by using the winding function method", *XIII International Conference on Electrical Machines (ICEM)*, pp. 2423–2429 (2018). DOI: 10.1109/ICELMACH.2018.8507049

8. Rezazadeh, G., Tahami, F., Capolino, G.A., et al. "Design of a six-phase squirrel cage induction motor with pseudo-concentrated windings", *International Conference on Electrical Machines (ICEM)*, pp. 2097–2103 (2021). DOI: 10.1109/ICEM49940.2020.9270682

9. Lin, C.H. and Hwang, C.C. "Multiobjective optimization design for a six-phase copper rotor induction motor mounted with a scroll compressor", *IEEE Transactions on Magnetics*, **52**(7), pp. 1–4 (2016). DOI: 10.1109/TMAG.2016.2517665

10. Apsley, J. and Williamson, S. "Analysis of multiphase induction machines with winding faults", *IEEE Transactions on Industry Applications*, **42**(2), pp. 465–472 (2006). DOI: 10.1109/IEMDC.2005.195731

11. Munim, W.N.W.A., Duran, M.J., Che, H.S., et al. "A unified analysis of the fault tolerance capability in six-phase induction motor drives", *IEEE Transactions on Power Electronics*, **32**(10), pp. 7824–7836 (2016). DOI: 10.1109/TPEL.2016.2632118

12. Mule, G.J.A., Munim, W.N.W.A., Tousizadeh, M., et al. "Post-fault tolerant of symmetrical six-phase induction machine under open circuit fault with single and two isolated neutral points using graphical user interface", In *AIP Conference Proceedings*, 020016 (2019). DOI:10.1063/1.5133931

13. Salem, A. and Narimani, M. "Fault-tolerant operation of asymmetrical six-phase motor drives in eV applications", In *IEEE Transportation Electrification Conference and Expo (ITEC)*, pp. 210–215 (2020). DOI: 10.1109/ITEC48692.2020.9161760

14. Alberti, L. and Bianchi, N. "Experimental tests of dual three-phase induction motor under faulty operating condition", *IEEE Transactions on Industrial Electronics*, **59**(5), pp. 2041–2048 (2011). DOI: 10.1109/TIE.2011.2171175

15. Pantea, A., Yazidi, A., Betin, F., et al. "Six-phase induction machine model for electrical fault simulation using the circuit-oriented method", *IEEE Transactions on Industrial Electronics*, **63**(1), pp. 494–503 (2015). DOI: 10.1109/TIE.2015.2493727

16. Chawla, R., Vinayak, B.A., and Jagadanand, G. "Modelling and detection of stator incipient open circuit fault in three-phase induction motor", In *IEEE International Conference on Power Electronics, Drives and Energy Systems (PEDES)*, pp. 1–6 (2018). DOI: 10.1109/PEDES.2018.8707681

17. Duran, M.J. and Barrero, F. "Recent advances in the design, modeling, and control of multiphase machines-Part II", *IEEE Transactions on Industrial Electronics*, **63**(1), pp. 459–468 (2015). DOI: 10.1109/TIE.2015.2448211

18. Yepes, A.G., Doval-Gandoy, J., Baneira, F., et al. "Postfault strategy for dual three-phase machines with minimum loss in the full torque operation range under two open phases", In *IEEE Energy Conversion Congress and Exposition (ECCE)*, pp. 3380–3385 (2018). DOI: 10.1109/ECCE.2018.8557522

19. Sala, G., Mengoni, M., Rizzoli, G., et al. "Impact of star connection layouts on the control of multiphase induction motor drives under open-phase fault", *IEEE*

Transactions on Power Electronics, **36**(4), pp. 3717–3726 (2020). DOI: 10.1109/TPEL.2020.3024205

20. Bramerdorfer, G. "Multiobjective electric machine optimization for highest reliability demands", *CES Transactions on Electrical Machines and Systems*, **4**(2), pp. 71–78 (2020). DOI: 10.30941/CESTEMS.2020.00011

21. Zagirnyak, M.V., Prus, V.V., Somka, O., et al. "Models of reliability prediction of electric machine taking into account the state of major structural units", *Advances in Electrical and Electronic Engineering*, **13**(5), pp. 71–78 (2015). DOI:10.15598/aeee.v13i5.1397

22. Li, W. and Cheng, M. "Investigation of influence of winding structure on reliability of permanent magnet machines", *CES Transactions on Electrical Machines and Systems*, **4**(2), pp. 87–95 (2020). DOI: 10.30941/CESTEMS.2020.00013

23. Giangrande, P., Madonna, V., Nuzzo, S., et al. "Moving toward a reliability-oriented design approach of low-voltage electrical machines by including insulation thermal aging considerations", *IEEE Transactions on Transportation Electrification*, **6**(1), pp. 16–27 (2020). DOI: 10.1109/TTE.2020.2971191

24. Li, W. and Cheng, M. "Reliability analysis and evaluation for flux-Switching permanent magnet machine", *IEEE Transactions on Industrial Electronics*, **66**(3), pp. 1760–1769 (2019). DOI: 10.1109/TIE.2018.2838105

25. Nandi, S., Toliyat, H.A., and Li, X. "Condition monitoring and fault diagnosis of electrical motors-A review", *IEEE Transactions on Energy Conversion*, **20**(4), pp. 719–729 (2005). DOI: 10.1109/TEC.2005.847955

26. Kliman, G.B., Premerlani, W.J., Koegl, R.A., et al. "A new approach to on-line turn fault detection in AC motors", In *IAS'96. Conference Record of the 1996 IEEE Industry Applications Conference Thirty-First IAS Annual Meeting*, pp. 687–693 (1996). DOI: 10.1109/IAS.1996.557113

27. Tavner, P.J. "Review of condition monitoring of rotating electrical machines", *IET Electric Power Applications*, **2**(4), pp. 215–247 (2008). DOI:10.1049/iet-epa:20070280

28. Nategh, S., Krings, A., Wallmark, O., et al. "Evaluation of impregnation materials for thermal management of liquid-cooled electric machines", *IEEE Transactions on Industrial Electronics*, **61**(11), pp. 5956–5965 (2014). DOI: 10.1109/TIE.2014.2308151

29. Jack, A.G., Mecrow, B.C., and Haylock, J.A. "A comparative study of permanent magnet and switched reluctance motors for high-performance fault-tolerant applications", *IEEE Transactions on Industry Applications*, **32**(4), pp. 889–895 (1996). DOI: 10.1109/28.511646

30. Alipour-Sarabi, R., Nasiri-Gheidari, Z., Tootoonchian, F., et al. "Analysis of winding configurations and slot-pole combinations in fractional-slots resolvers", *IEEE Sensors Journal*, **17**(14), pp. 4420–4428 (2017). DOI: 10.1109/JSEN.2017.2707523

31. Toliyat, H.A., Nandi, S., Choi, S., et al., *Electric Machines: Modeling, Condition Monitoring, and Fault Diagnosis*, CRC Press (2017). DOI:10.1201/b13008

32. Kaboli, S., *Reliability in Power Electronics and Electrical Machines: Industrial Applications and Performance Models: Industrial Applications and performance models*, IGI Global (2016). DOI: 10.4018/978-1-4666-9429-3

33. Lin, J., Cheng, L., Chang, Y., et al. "Reliability based power systems planning and operation with wind power integration: A review to models, algorithms and applications", *Renewable and Sustainable Energy Reviews*, **31**(1), pp. 921–934 (2014). DOI: 10.1016/j.rser.2013.12.034

34. Billinton, R. and Allan, R.N., *Reliability Evaluation of Engineering Systems*, Springer (1992). DOI:10.1007/978-1-4899-0685-4

Biographies

Mehdi Alemi-Rostami was born in Behashahr, Iran, in 1980. He received his BSc degree from Gilan University, Gilan, Iran, in 1998, and his MS and PhD degrees from Iran University of Science and Technology, Tehran, Iran, in 2000 and 2011, respectively, all in power electronics. He is currently an Assistant Professor at the Khayam Research Institute (KRI), Ministry of Science, Research, and Technology, Tehran, Iran.

Ghasem Rezazadeh was born in Freydoonkenar, Iran, in 1990. He received his BS degree in electrical engineering from Shahid Beheshti University in 2012. In 2014, he received his MSc degree from Sharif University of Technology, Tehran, Iran. He received his PhD degree in a co-supervision between Sharif University of Technology and the University of Picardie "Jules Verne", Amiens, France. His research interests include electrical machine design, modeling, and drive.

Farzad Tahami received his BS degree in electrical engineering from Ferdowsi University of Mashhad, Mashhad, Iran, in 1991, and his MS and PhD degrees in electrical engineering from the University of Tehran, Tehran, Iran, in 1993 and 2003, respectively. From 1991 to 2004, he was with the *R&D* department of Jovain Electrical Machines Corporation (JEMCO), Iran. In 2004, he joined Sharif University of Technology, Tehran, Iran, where he is currently an Associate Professor. Since 2007, he has been the Chairman of the technical committee of rotating machinery at the Iranian National Electrotechnical Committee (INEC). Dr. Tahami is a Member of the Board of Directors and the Chairman of the education committee of the Power Electronics Society of Iran (PESI). His current research interests include electric motor drives, modeling and control of power electronic converters, soft switching, resonant converters, and wireless power transfer.

Hamid Reza Akbari-Resketi was born in Sari, Iran, in 1992. He received his MSc degree in electrical power engineering from the Babol Noshirvani University of Technology, Babol, Iran in 2019. His research interests include design, simulation, optimization, control, and performance analysis of electrical machines.